The Effects of Subgrid Model Mixing and Numerical Filtering in Simulations of Mesoscale Cloud Systems

TETSUYA TAKEMI* AND RICHARD ROTUNNO

National Center for Atmospheric Research,+ Boulder, Colorado

(Manuscript received 19 April 2002, in final form 27 February 2003)

ABSTRACT

Using the newly developed Weather Research and Forecasting (WRF) model, this study investigates the effects of subgrid mixing and numerical filtering in mesoscale cloud simulations by examining the sensitivities to the parameters in turbulence-closure schemes as well as the parameters in the numerical filters. Three-dimensional simulations of squall lines in both no-shear and strong-shear environments have been performed. Using the Smagorinsky or 1.5-order turbulent kinetic energy (TKE) subgrid model with standard values for the model constants and no explicit numerical filter, the solution in the no-shear environment is characterized by many poorly resolved grid-scale cells. In the past, such grid-scale noise was avoided by adding a numerical filter which, however, produces excessive damping of the physical small-scale eddies. Without using such a filter, it was found that by increasing the proportionality constant in the eddy viscosity coefficient in the subgrid turbulence models, the cells become well resolved, but that further increases in the constant overly smooth the cells. Such solution sensitivity is also found in the strong-shear cases. The simulations using the subgrid models with viscosity coefficients 1.5 to 2 times larger than those widely used in other cloud models retain more power in short scales, but without an unwanted buildup of energy; with these optimum values, no numerical filters are required to avoid computational noise. These optimum constants do not depend significantly on grid spacings of O(1 km). Therefore, it is concluded that by using the eddy viscosity formulation appropriate for mesoscale cloud simulations, the use of artificial numerical filters is avoided, and the mixing processes are represented by more physically based turbulence-closure models.

1. Introduction

Mesoscale cloud models employ a turbulence closure model in order to represent subgrid-scale (SGS) effects. The turbulence-closure models widely used in cloud models, such as the Klemp–Wilhelmson model (Klemp and Wilhelmson 1978), the Advanced Regional Prediction System (ARPS; Xue et al. 1995), and the Coupled Ocean–Atmosphere Mesoscale Prediction System (COAMPS; Hodur 1997), are either a Smagorinsky-type first-order-closure scheme, or a one-and-one-half-order scheme using a prognostic equation of turbulent kinetic energy (TKE). In addition to the SGS mixing, a small amount of background mixing is often employed in order to suppress small-scale computational noise originating in finite-difference schemes. A common way to achieve the background mixing is to add an artificial scale-selective spatial filter to the model equations. The higher the order of the filter, the stronger is the scale selectivity. However, these filters cannot differentiate between the physical modes and computational noise, and damp all small-scale perturbations. In some cases physically meaningful small-scale eddies may be suppressed, which can impact the development of mesoscale cloud systems. Therefore, an assessment of subgrid mixing and numerical filtering is crucial for ensuring that a cloud simulation is successful.

The two turbulence-closure models mentioned earlier are formulated as follows: The Smagorinsky-type scheme, in the version proposed by Lilly (1962), defines the eddy viscosity coefficient K_m as

$$K_m = (C_s\Delta)^2|S|\sqrt{1 - \frac{\mathrm{Ri}}{\mathrm{Pr}}}, \tag{1}$$

where

$$S^2 = \frac{1}{2}\left(\frac{\partial u_i}{\partial x_j} + \frac{\partial u_j}{\partial x_i}\right)^2. \tag{2}$$

Here C_s is constant, Δ a measure of the grid scale, Ri the Richardson number, and Pr the turbulent Prandtl

* Additional affiliation: Department of Global Architecture, Osaka University, Osaka, Japan.

+ The National Center for Atmospheric Research is sponsored by the National Science Foundation.

Corresponding author address: Dr. Tetsuya Takemi, Department of Global Architecture, Osaka University, Graduate School of Engineering, 2-1 Yamadaoka, Suita, Osaka 565-0871, Japan.
E-mail: takemi@ga.eng.osaka-u.ac.jp

number. In the TKE scheme (e.g., Klemp and Wilhelmson 1978), the eddy viscosity coefficient is given by

$$K_m = C_k e^{1/2} l, \tag{3}$$

where C_k is a constant, e is the turbulent kinetic energy, and l a length scale. The TKE scheme needs another diagnostic equation to close the TKE equation, which is for the dissipation rate of TKE and given by

$$\epsilon = \frac{C_e e^{3/2}}{l}, \tag{4}$$

where C_e is a constant. The length scale l in (3) and (4) is defined based on the grid scale. In these SGS models, one must determine the proportionality constants C_s and C_k for the eddy viscosity coefficient, and the proportionality constant C_e for the TKE dissipation rate. The values for these constants were derived from theoretical considerations for inertial-subrange, locally isotropic turbulence (Lilly 1966), and have been widely used for simulations of boundary layer flows (e.g., Deardorff 1972, 1980; Moeng 1984).

The effects of subgrid mixing and numerical errors have been investigated for large-eddy simulations of turbulent boundary layer flows (e.g., Mason and Callen 1986; Kravchenko and Moin 1997; Mason and Brown 1999; Glendening and Haack 2001). Extensive studies using the Smagorinsky model have been done by Mason and his colleagues. Mason and Callen (1986) viewed C_s as a measure of numerical accuracy, a ratio of a mixing-length scale l_0 to a grid scale, that is, $C_s = l_0/\Delta$. They found that at a fixed grid spacing the results of the simulations showed a strong dependence on C_s: larger C_s gives flows with smoothed features, while reducing C_s suffers from grid-scale perturbations. By examining such sensitivity, Mason (1994) concluded that the constant $C_s \sim 0.2$ gives an optimum solution in which the finite-difference error is small and the simulated eddies are well resolved. Mason and Brown (1999) confirmed Mason and Callen's finding and showed that at a fixed mixing-length scale l_0 a simulation with larger C_s (i.e., higher resolution) gives a more reasonable solution. Canuto and Cheng (1997) concluded that C_s is not a constant but a dynamical variable, which is adjusted depending on different flows. In this way, the Smagorinsky constant C_s cannot be regarded as a universal constant. The eddy viscosity in the Smagorinsky scheme can be easily derived from the TKE prognostic equation (e.g., Sullivan et al. 1994); thus, Mason's (1994) argument would also apply to the eddy viscosity formulation in the TKE scheme, and so, to cloud simulations.

The effects of numerical filter (artificial diffusion) on storm simulations have been discussed by Lilly and Jewett (1990) and Weisman et al. (1997). Lilly and Jewett analyzed simulated supercell thunderstorms produced by the Klemp–Wilhelmson model, and showed that the artificial filter had much more effect on the simulations than the more physically based mixing provided by SGS closure. Weisman et al. obtained similar results, and also reported that reducing the numerical filter results in grid-scale storms. These studies, however, were not able to separate the subgrid mixing and numerical filters because the numerical model used could not be run to simulate convection without a numerical filter.

In this study, we investigate the effects of subgrid model mixing and numerical filtering in mesoscale cloud simulations whose grid sizes are on the order of 1 km (probably far from the inertial subrange), using a newly developed mesoscale cloud model, the Weather Research and Forecasting (WRF) model (Skamarock et al. 2001). For this purpose, we examine the sensitivities of the simulated cloud systems to the SGS constants C_s, C_k, and C_e as well as filter strength. We also examine the sensitivities to the grid spacing for a selected combination of SGS constants. To our knowledge, this is the first attempt to investigate systematically such effects in mesoscale cloud simulations. We will address some problems of employing SGS schemes (which were originally developed for simulation of turbulence and turbulent boundary layer flows) for cloud models, and suggest possible solutions that do not depend on numerical filters. The simulations are performed on squall lines in an idealized situation, which have been extensively investigated in the literature (e.g., Rotunno et al. 1988; Weisman et al. 1988).

2. Model and experimental design

a. The model, numerical filters, and subgrid model constants

Numerical simulations are performed using the WRF model, a newly developed compressible nonhydrostatic cloud model. The basic equations and the description of the numerics can be found in Skamarock et al. (2001) and Wicker and Skamarock (2002). In the WRF model, a third-order-accurate Runge–Kutta scheme is used for the time integration, and second- to sixth-order-accurate spatial-discretization schemes are available for the advection terms. Among these spatial differencings, the third-order and fifth-order schemes are upwind-biased so as to make the model more computationally stable than would be the case using the even-order centered-differencing schemes; this is because the upwind discretizations have built-in high-order diffusive filters with a coefficient proportional to the local Courant number (Wicker and Skamarock 2002). There are other damping terms in the model: divergence damping of acoustic energy (Skamarock and Klemp 1992), and computational damping built into the Runge–Kutta time integration scheme. All these implicit damping terms allow the model to run stably without any additional artificial spatial dissipation, such as a fourth-order diffusion, which in many other cloud models is unavoidable. In this study, we refer to an artificial and explicit spatial dissipation as a numerical filter.

Many cloud models such as the Klemp–Wilhelmson

model, ARPS, and COAMPS use a fourth-order diffusion (only in the horizontal directions) as a numerical filter to suppress very short wavelength modes. Thus, we also have added a fourth-order diffusion to the WRF model as a numerical filter in order to examine the effects of the filter. Klemp and Wilhelmson (1978) suggested the use of the nondimensional filter coefficient $K_4 = 2.5 \times 10^{-3}$ in order to keep the physical modes relatively unaffected. According to this, we use the filter coefficient $K_4 = 2.4 \times 10^{-3}$ as a weak filter (referred to as FILTER1 in this study) and, for comparison, $K_4 = 1.2 \times 10^{-2}$ as a strong filter (referred to as FILTER2).

The subgrid models used in the present study are the Smagorinsky and TKE schemes. As mentioned in the introduction, the SGS constants were derived theoretically by Lilly (1966), which are $C_s = 0.23$, $C_k = 0.12$, and $C_e = 0.68$. The ARPS model uses $C_s = 0.21$ after Deardorff (1972). Most boundary layer and cloud models employing the TKE scheme use $C_k = 0.1$, while Klemp and Wilhelmson (1978) used $C_k = 0.2$. Several values were used for C_e in cloud and boundary layer simulations: 0.2 in Klemp and Wilhelmson (1978); and 0.7 in Deardorff (1980) (including the effect of stability). Moeng and Wyngaard (1988) compared spectra from numerical simulations with those from theoretical predictions and found that those constants are $C_k = 0.1$ and $C_e = 0.93$ if the grid spacing is within the inertial subrange; they also found that the simulations of a convective boundary layer are insensitive to modest changes in these constants. Here, we refer to $C_s = 0.2$ and $C_k = 0.1$ as the base SGS constants and examine the influence of varying these constants upon squall-line simulations. We also examine the sensitivities of changing C_e mainly to 0.2, 0.7, and 0.93.

In (1) and (3), a length scale must be determined; we define both Δ and l as the geometric-average grid spacing: $(\Delta x \Delta y \Delta z)^{1/3}$, following Klemp and Wilhelmson (1978). Deardorff (1980) defined the length scale as a function of stability: if the stability becomes large the length scale becomes smaller than the average grid spacing; this formulation has often been employed in cloud models. If the length scale is some function of stability, eddy viscosity varies depending not only on C_k and e but also on l. This definition, however, makes the scheme a little more complicated; thus, we use a constant length scale in order to simplify the interpretation of the results.

The relationship between the Smagorinsky constant C_s and the TKE constants C_k and C_e can be derived following Sullivan et al. (1994). Including the effect of buoyancy production of TKE in their derivation, and considering an equilibrium balance between the shear and buoyancy production terms and the dissipation term in the prognostic TKE equation, we can obtain

$$C_s = \left(\frac{C_k^3}{C_e}\right)^{1/4}. \tag{5}$$

This equation states that increasing C_k or decreasing C_e corresponds to increasing C_s. If C_s becomes larger, eddy viscosity in (1) becomes larger and thus smoothing is expected to be larger. With this relationship as a guide, we can expect some correspondence between the results obtained with the Smagorinsky and TKE schemes.

b. Experimental design

The present study mainly focuses on the squall-line evolution in a no-shear environment, which would result in less organized convective cells near the squall-line cold outflow boundary. The model is run in a three-dimensional domain of 300 km in the x (across-line) direction and 80 km in the y (along-line) direction extending from the surface to a height of 18 km. The grid resolution of the simulations is 1 km in the horizontal direction and 500 m in the vertical direction (except for those simulations described in section 3e). In section 3e, results with different horizontal grid spacings, that is, 500 m, 2, and 4 km, are presented. The model is integrated up to 4 h, at which time the squall-line cold outflow boundary is still within the computational domain. The third-order Runge–Kutta scheme is used for the time integration. The WRF model employs the time-splitting method of Klemp and Wilhelmson (1978), and in this study the large time step is set to 6 s (3 s only for the case with the 500-m horizontal grid spacing) with four small time steps within a single large time step. The domain size in the y direction is smaller than those of the simulations by Rotunno et al. (1988) and the recent simulations by Weisman and Rotunno (2001). This smaller domain size has been used because our test case, squall-line evolution in a no-shear environment, has no systematic variability on scales longer than a few tens of kilometers in the along-line direction. Open lateral boundary conditions are specified at the x boundaries, and periodic conditions at the y boundaries. The top boundary is a rigid lid with an absorbing layer in the upper 6-km depth, while the bottom boundary is free slip. In the present idealized simulations, the Kessler warm-rain scheme is used for microphysics parameterization, and the Coriolis parameter is set to zero.

A horizontally uniform thermodynamic environment has been created by the analytic profile of Weisman and Klemp (1982), which is a typical condition for strong midlatitude convection. The water vapor mixing ratio in the boundary layer is set to 14 g kg^{-1}. Two initial wind profiles are used: no shear, no flow; and the unidirectional shear of 20 m s^{-1} in the lowest 2.5 km, which Rotunno et al. (1988), Weisman et al. (1988), and Weisman and Rotunno (2001) have considered. Squall lines are initiated by a y-oriented line thermal (a 1.5-K-maximum potential temperature excess) of across-line radius of 10 km and vertical radius of 1.5 km, placed at the domain center and at a height of 1.5 km. Small random potential temperature perturbations of less than 0.1 K

are added to this thermal in order to accelerate the tendency toward three-dimensionality.

We use the third-order upwind-differencing scheme for the vertical advection terms in all the simulations described here. For the horizontal advection terms, we compare three different numerical treatments: third-order upwind, fourth-order centered, and fifth-order upwind schemes.

3. Squall-line simulations in no shear

a. Base SGS constants cases

The simulations employing the base SGS constants ($C_s = 0.2$ and $C_k = 0.1$) are considered first to address the issue of using subgrid models without any numerical spatial filters. The fifth- and third-order upwind schemes are used for the horizontal advection discretization.

The initial line thermal in the no-shear environment produced a cold pool spreading toward both sides in the *x* direction. Weak updrafts were forced at the gust front, which developed into cloud cells, but the updrafts at the gust front were not strong enough to make these cells deeply developed at the front; rather, the cells were advected rearward of the gust front and turned into deep, more or less randomly distributed cells behind the front.

Figure 1 shows the horizontal cross section of vertical velocity at the 3-km level and the surface outflow boundary at 4 h in a 40 km × 40 km area near the right-moving outflow. The subgrid models used here are the Smagorinsky and TKE schemes, and the fifth-order scheme is used for the horizontal advection discretization. The explicit numerical filters are not used in these simulations. As clearly seen in Fig. 1, in both the Smagorinsky and TKE schemes, grid-scale features are widespread behind the gust front, and no well-resolved cells are found. We have performed the same simulations as in Fig. 1, which instead employed the third-order scheme for the advection differencing (Fig. 2), and, as can be seen, there are fewer grid-scale features in the solutions.

The more smoothed fields seen in the third-order scheme simulations are due to the stronger implicit dissipation in the third-order upwind-differencing scheme than in the fifth-order scheme, but this stronger implicit filtering only masks the problem revealed in Fig. 1 (see the appendix for the formulations and characteristics of these implicit filters). Wicker and Skamarock (2002) examined the accuracy of high-order schemes for advection discretization along with a variety of time-differencing schemes, and, among the possibilities they considered, found that the fifth-order upwind scheme combined with the third-order Runge–Kutta time integration scheme provides the smallest error in a one-dimensional advection test of a single pulse. They also performed two-dimensional simulations of cold air descending and obtained the most satisfactory solution (i.e., no grid-scale oscillations) using a combination of

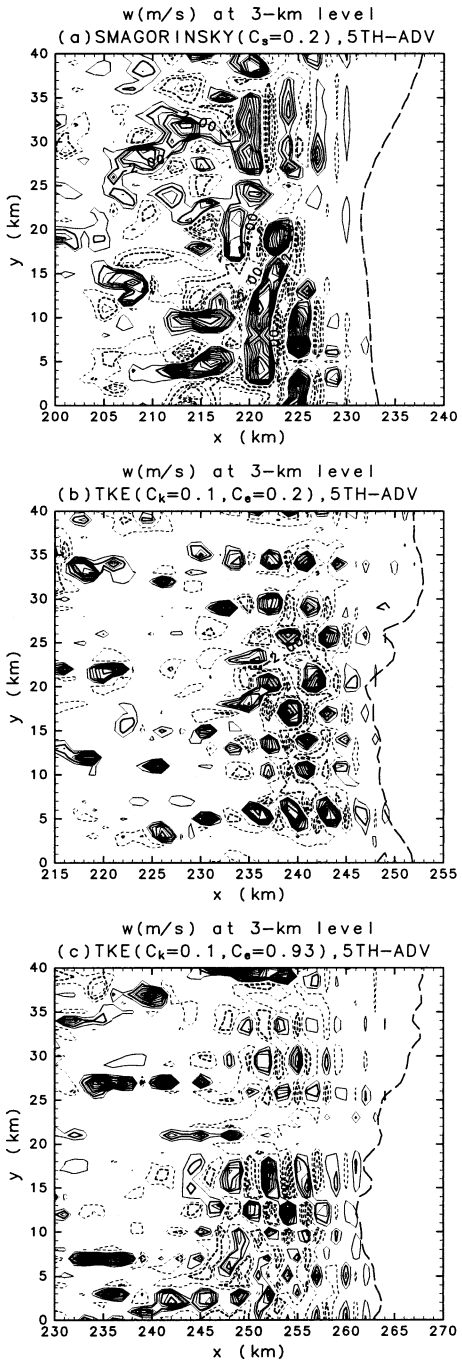

FIG. 1. Horizontal cross section of vertical velocity at the height of 3 km, contoured at a 1 m s^{-1} interval after 4 h of simulation. The simulations are conducted using the fifth-order upwind scheme for the horizontal advection discretization. The gust front is also indicated by long-dashed lines. (a) Smagorinsky scheme with $C_s = 0.2$, (b) TKE scheme with $C_k = 0.1$ and $C_e = 0.2$, and (c) TKE scheme with $C_k = 0.1$ and $C_e = 0.93$. A 40 km by 40 km portion of the entire domain is shown. (a), (b), (c) Note that the *x* coordinate is different in each.

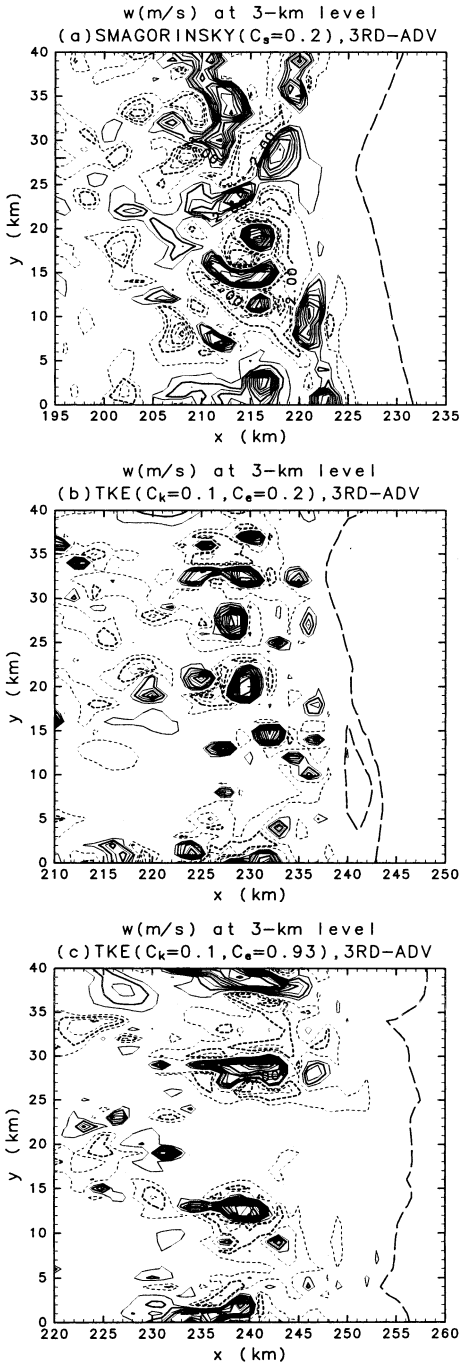

FIG. 2. Same as in Fig. 1 except for using the third-order upwind scheme for the horizontal advection discretization.

the fifth-order spatial and third-order Runge–Kutta time-differencing schemes with a minimum amount of background mixing (second-order filter). Thus, it might be expected that the combination of the fifth-order upwind and third-order Runge–Kutta schemes would also provide the most accurate solution in the present squall-line simulations, in which many poorly resolved cells were produced. Hence the question raised by Figs. 1 and 2 is the following: Why does the use of a higher-order scheme allow such a noisy result?

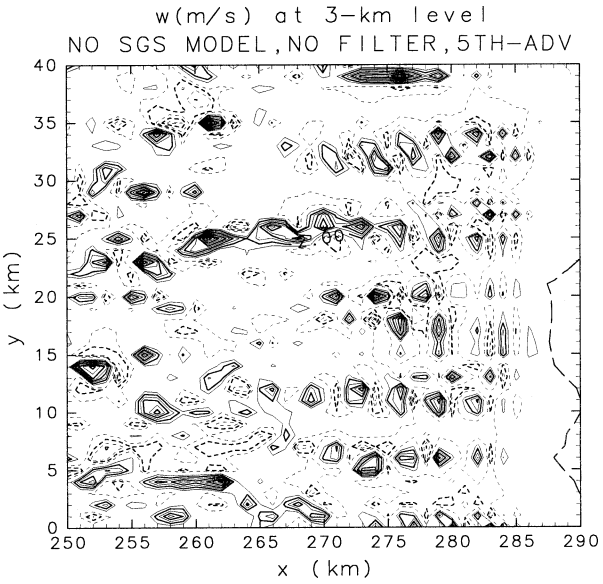

FIG. 3. Same as in Fig. 1 except for employing no subgrid model nor additional filter.

In order to examine the cause of the grid-scale features seen in Fig. 1, we have performed a simulation employing neither subgrid model nor additional filter with the fifth-order advection scheme. It should be noted that such a simulation can be conducted because of implicit dissipation in the WRF model, while other cloud models employing a centered-differencing scheme for advection terms cannot be run stably without any additional artificial dissipations. Figure 3 shows that grid-scale erroneous featuers are also seen in this simulation. Comparing Figs. 1 (with subgrid model) and 3 (without subgrid model), the simulated fields look similar to each other, especially Fig. 3 to Fig. 1c (the result obtained with $C_k = 0.1$ and $C_e = 0.93$); thus, the grid-scale noise seen in Fig. 1 results from the erroneous features simulated with neither physical nor numerical dissipation. It can be said that the fifth-order scheme is useful for making the model computationally stable but the implicit smoothing is not enough to control the physical tendency for rapid growth of convective energy on the smallest scales. Thus, the mixing by subgrid models needs to work appropriately in order to represent such cells; however, the simulations suggest that the subgrid mixing is not large enough to produce well-resolved cells, and thus the grid-scale noise becomes dominant.

There are no explicit numerical filters in the simulations shown in Fig. 1, so one way to avoid the noisy solution has been to add a fourth-order filter. This is still commonly used in many cloud models that employ leapfrog-time and centered-spatial differencing schemes. However, a numerical filter is an artificial smoother and affects not only numerical errors but also small-scale physical eddies. Instead of employing such

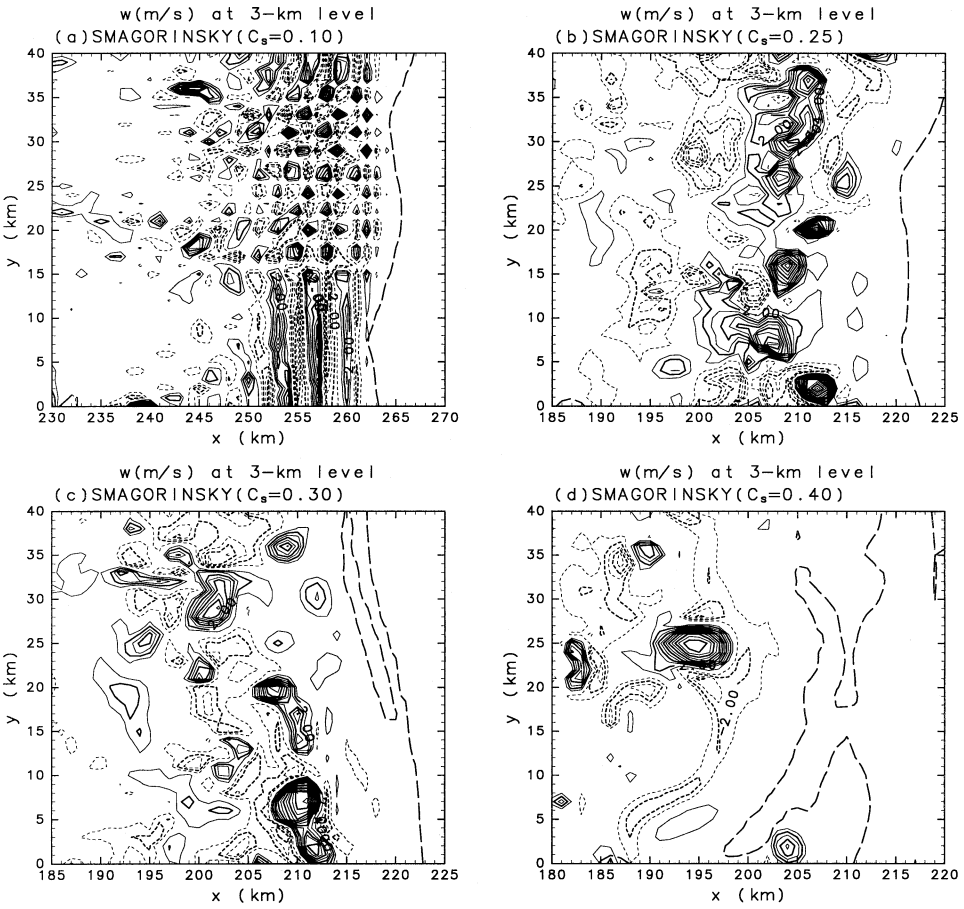

FIG. 4. Same as in Fig. 1 except for the Smagorinsky scheme with (a) $C_s = 0.1$, (b) $C_s = 0.25$, (c) $C_s = 0.3$, and (d) $C_s = 0.4$.

an artificial filter, we seek to find another way to avoid the grid-scale noise by examining the effects of subgrid model mixing and numerical filtering in squall-line simulations.

b. Sensitivities to SGS constants

Hereafter, the fifth-order upwind scheme is used for the simulations unless otherwise stated.

First, the effects of varying C_s and C_k are examined. Figures 4 and 5 show the horizontal cross section of vertical velocity at the 3-km level around the right-moving cold surface outflow at 4 h. Employing the Smagorinsky scheme with smaller C_s (=0.1) than used in the case shown in Fig. 1a, the result looks much worse; more grid-scale ''diamonds'' can be seen. On the other hand, increasing the constants C_s and C_k beyond the base values, the cells become smoother and well represented; the cells look well resolved above $C_s = 0.25$ (Fig. 4b) for the Smagorinsky scheme and $C_k = 0.2$ (Fig. 5b) for the TKE scheme. When the constants are further increased, the cells look even smoother (Figs. 4c,d and 5c,d). The more smoothed cells produce less rainfall and thus less evaporative cooling, which results in weaker cold pools. Since the movement of the cold pool is related to the cold pool intensity, the position of the gust front (defined as the position where the potential temperature perturbation at the lowest level is -1 K) obtained with larger C_s and C_k is behind that obtained with the smallest C_s and C_k (note that the x coordinate is different from panel to panel). These features were also found in the TKE schemes using other C_e values. From Fig. 4 we see that the results obtained with $C_s = 0.25 \sim 0.3$ appear to be satisfactory for the Smagorinsky scheme; Fig. 5 indicates that the simulations with $C_k = 0.2 \sim 0.25$ would be satisfactory for the TKE scheme with $C_e = 0.93$. Our tests using the TKE scheme with $C_e = 0.2$ (not shown) indicates $C_k = 0.15 \sim 0.2$ also gives satisfactory solutions.

To compare more systematically the system-scale features of the simulations, the total rainfall and the power spectral density are calculated. The total rainfall (integrated over the entire domain and over 1–4 h) is summarized in Table 1. Generally, the total rainfall gradually decreases with increasing values of the constant C_s or C_k in all the subgrid models. It is noted that at a fixed

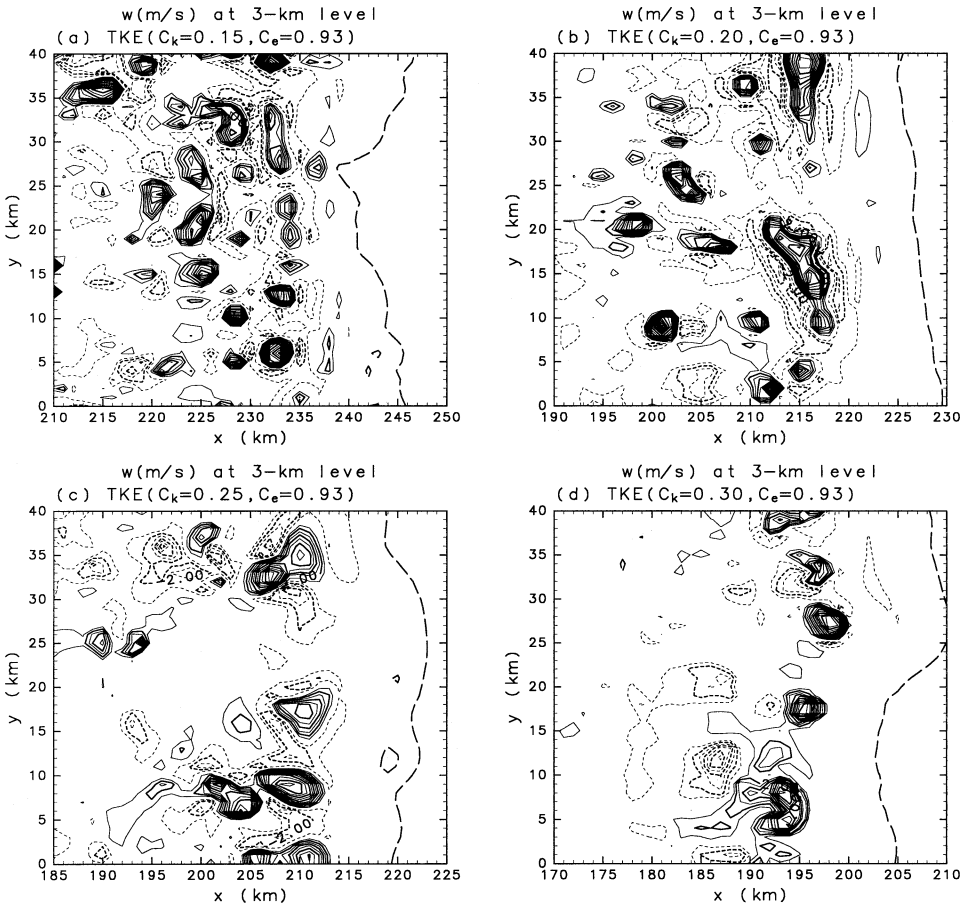

FIG. 5. Same as in Fig. 1 except for the TKE scheme ($C_e = 0.93$) with (a) $C_k = 0.15$, (b) $C_k = 0.2$, (c) $C_k = 0.25$, and (d) $C_k = 0.3$.

C_k the rainfall increases with increasing the constant C_e. This can be interpreted by considering Eq. (5): C_e is inversely proportional to C_s at a fixed C_k. Thus, increasing C_e corresponds to decreasing C_s, which means less smoothing and thus more rainfall. This C_e dependence is also described later in this section. In Table 1, it is also noted that the rainfall obtained with $C_e = 0.2$ agrees well with that obtained with $C_e = 0.93$ but a larger C_k [cf. $(C_k, C_e) = (0.15, 0.2)$ with $(C_k, C_e) = (0.2, 0.93)$ and $(C_k, C_e) = (0.2, 0.2)$ with $(C_k, C_e) = (0.25, 0.93)$]. This agreement is also expected from (5): C_k is proportional to C_e at a fixed C_s. Thus, the result obtained with smaller C_k and C_e will be similar to that obtained with larger C_k and C_e.

TABLE 1. Domain total rainfall between 1 and 4 h in no-shear cases simulations obtained with the Smagorinsky (SMAG) and TKE schemes ($C_e = 0.2$, $C_e = 0.7$, and $C_e = 0.93$).

C_s or C_k	Total rainfall ($\times 10^{12}$ kg)			
	SMAG	$C_e = 0.2$	$C_e = 0.7$	$C_e = 0.93$
0.1	0.128	0.120	0.132	0.135
0.15	—	0.104	0.115	0.115
0.2	0.119	0.0899	0.0979	0.0990
0.25	0.127	0.0834	0.0894	0.0904
0.3	0.115	0.0752	0.0760	0.0819
0.4	0.0793	—	—	—

Power spectral density in the across-line (x) and along-line (y) directions was computed for the vertical velocity at the 3-km level in a 80 km $\times$ 80 km area around the rightward-moving surface outflow. The right boundary of this computation area was determined at a position 20 km ahead of the gust front. The spectra in each direction were calculated in the domain at each model output time, and averaged over the domain; then the domain-averaged one-dimensional spectra were averaged over the last hour of the simulation (the data time interval is 15 min). Figure 6 shows the power spectral densities in the across-line direction obtained employing the Smagorinsky scheme with C_s varying from 0.1 to 0.4. A $-5/3$ slope, which is expected in an inertial subrange for three-dimensional locally isotropic turbulence, is also plotted in the figure for reference. With $C_s = 0.1$ and 0.2, there is a significant energy buildup at short wavelengths (3–4 Δx waves). However, with $C_s \geq 0.25$ there is no such buildup of energy at short scales. The spectral slopes at short wavelengths

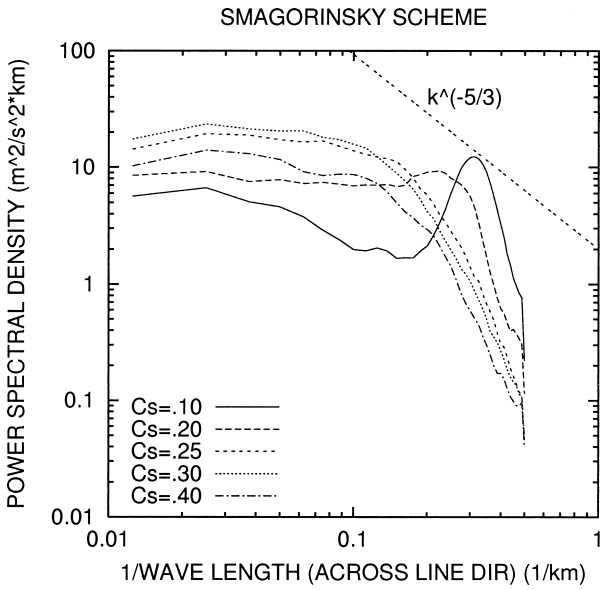

FIG. 6. Power spectral density of vertical velocity at the 3-km level for across-line (x) direction obtained using the Smagorinsky scheme with various C_s values. A $k^{-5/3}$ line is also plotted for reference.

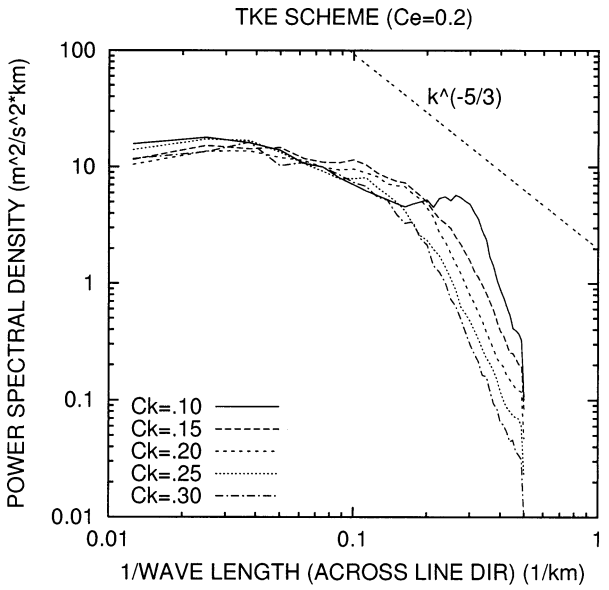

FIG. 7. Same as in Fig. 6 except for cases with the TKE scheme ($C_e = 0.2$) for various C_k values.

more rapidly decrease with wavenumber than the $-5/3$ dependence. The steep falloff at short wavelengths was also observed in large-eddy simulations of the planetary boundary layer (Mason and Brown 1999). These slopes steeper than the $-5/3$ line can be affected by both the smoothing characteristic implied by the Smagorinsky model, which is quite similar to Gaussian-type filter (Pope 2000, 590–594), and the implicit filtering in the upwind advection scheme (see the appendix).

Figure 7 shows the power spectral densities of vertical velocity as in Fig. 6 but with the TKE scheme ($C_e = 0.2$ cases) in the across-line direction. The spectra at short wavelengths look similar to those shown in Fig. 6. A spurious buildup of energy is seen in the $C_k = 0.1$ case; however, with $C_k \geq 0.15$ the power in short scales (wavelength less than $10\Delta x$) smoothly decreases with increasing wavenumber without any buildup of energy. At a fixed wavenumber in the short scales, the power decreases with increasing C_k. In Fig. 8, power spectra in the across-line direction are shown for the TKE scheme with $C_e = 0.93$, and the same behavior as shown in Fig. 7 ($C_e = 0.2$) can be seen.

To see the difference of the simulated field obtained with the different C_e values, the horizontal cross sections for the $C_e = 0.2$ and 0.7 cases with $C_k = 0.2$ (Fig. 9) are compared with that shown in Fig. 5b. As C_e decreases, the simulated field becomes smoother and small-scale features disappear. In Fig. 10 the power spectra for the $C_k = 0.2$ cases with the three C_e values are shown for both the across-line and along-line directions. Consistent with the behavior shown in Fig. 9, the power in short scales decreases with decreasing C_e. These results are also consistent with the trend of decreasing total rainfall with decreasing C_e (Table 1) for a given C_k.

Considering the smoother field with smaller C_e, one might expect that the simulation looks satisfactory even with $C_k = 0.1$ if C_e is further reduced. To examine this, we have performed simulations with C_e further reduced to $C_e = 0.12$ [which gives $C_s = 0.3$ from (5)] and $C_e = 0$ (as a limit case), along with $C_k = 0.1$, and obtained basically the similar features as shown in Figs. 1b,c (figure not shown). In Fig. 11, power spectra for the cases with $C_e = 0.93$, 0.12, and 0 are shown. Energy

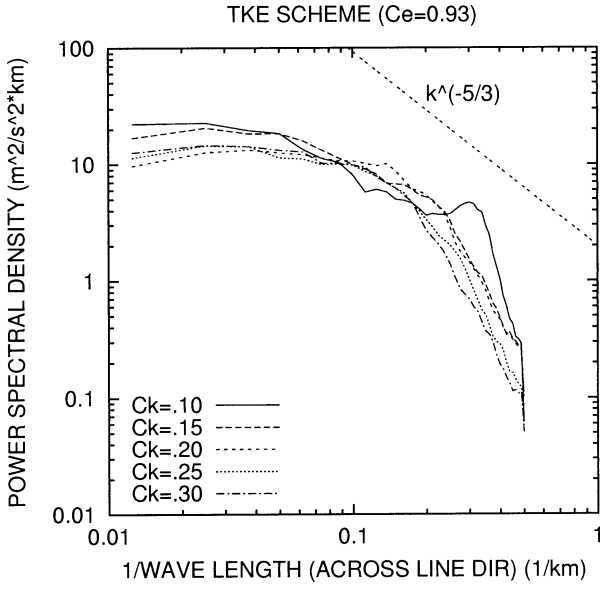

FIG. 8. Same as Fig. 6 except for cases with the TKE scheme ($C_e = 0.93$) for various C_k values.

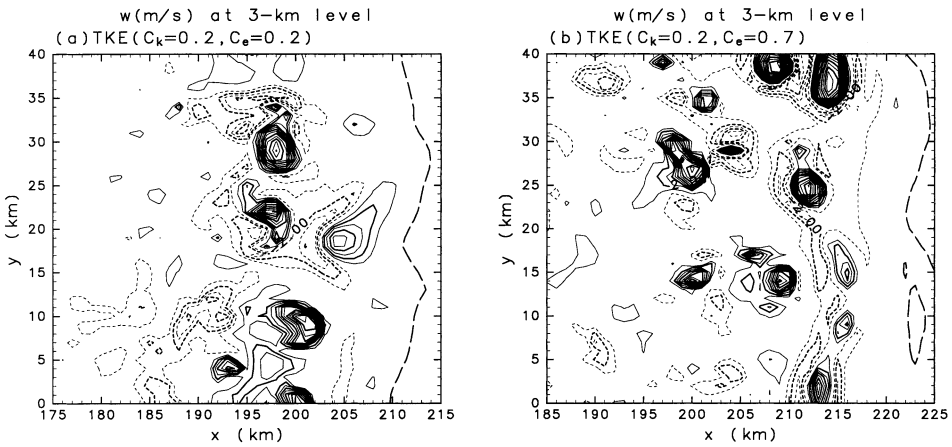

FIG. 9. Same as in Fig. 1 except for the TKE scheme with $C_k = 0.2$ and (a) $C_e = 0.2$, and (b) $C_e = 0.7$.

buildup in short scales can be seen for all the C_e values. Thus, although some sensitivity to the C_e value has been noted in Figs. 9 and 10, the effects of changing C_e are smaller than those of changing C_k.

It is noted that the case $C_e = 0$ may appear to be problematic since in this case there is no dissipation and therefore ever-increasing volume-integrated TKE. Our examination of both the domain-integrated and point values of the TKE in the previous cases (not shown) indicates that the local maximum values of TKE became only slightly larger as C_e was reduced, and remained finite even in the limit of $C_e = 0$ [maximum TKE ($C_e = 0$) ~ 60 m^2 s^{-2}; maximum TKE ($C_e = 0.93$) ~ 30 m^2 s^{-2}]. Our analysis indicates that since the turbulence associated with cumulus convection is confined to a small portion of the domain, the increasing domain-integrated TKE signifies that TKE produced in association with the convective cells is subsequently advected and diffused over an increasing volume and does not necessarily imply drastically larger point values.

c. Sensitivities to numerical schemes

Next, the sensitivities to the discretization schemes for the horizontal advection terms are examined. The schemes used here are third-order upwind, fifth-order upwind, and fourth-order centered-differencing schemes. In order to compare these schemes with a commonly used scheme in other cloud models, the fourth-order centered scheme along with FILTER1 is also examined. The subgrid model used here is the TKE scheme with (C_k, C_e) = (0.2, 0.2). We have also conducted simulations with the base constant $C_k = 0.1$, but the computation using the fourth-order scheme without a numerical filter was very unstable and soon stopped.

Figure 12 shows the power spectral densities of vertical velocity, as in Fig. 6, using the various differencing schemes. Among the four spectra, the slope with the fourth-order scheme differs the most from the other three; the power at short wavelengths (4–10Δx) is largely lost as compared to that with the upwind schemes, while the power at the shortest wavelengths (less than 4Δx) is relatively retained. Comparing the power in the 4–10Δx waves, the fifth-order scheme retains more energy. A better result can be obtained using the third-order scheme than using the fourth-order scheme. In the case of the fourth-order scheme with FILTER1 the power at short scales is significantly lost. It is noted that the difference between the spectra of the two upwind schemes is small. Consistent with this, the difference between the domain total rainfall obtained with the two schemes is also small: 0.0899×10^{12} kg for the fifth-order scheme (Table 1); and 0.0855×10^{12} kg for the third-order scheme.

From these results we can conclude that the use of the fifth-order scheme is the best choice in the sense that more power is retained at short scales.

d. Sensitivities to numerical filters

To examine the effects of numerical filters, the simulations employing the TKE scheme along with fourth-order filters and, for comparison, employing no subgrid model but only a numerical filter have been performed. The SGS constants are $C_k = 0.1$ and $C_e = 0.93$. The fifth-order differencing scheme is used for the advection terms.

Figure 13 shows the horizontal cross section of vertical velocity at the 3-km level. Adding the weak filter (FILTER1; Fig. 13a), the noise as seen in Fig. 1c is under control, and the cells appear to be smoothed. Using the stronger filter (FILTER2; Fig. 13b), the simulated cells become further smoothed and most of the small-scale features seen in Fig. 13a disappear (Fig. 13b). It is very interesting to compare the results obtained with and without the TKE scheme (Figs. 13a and 13c); the degree of smoothness of the well-resolved cells looks similar to each other. This indicates that adding

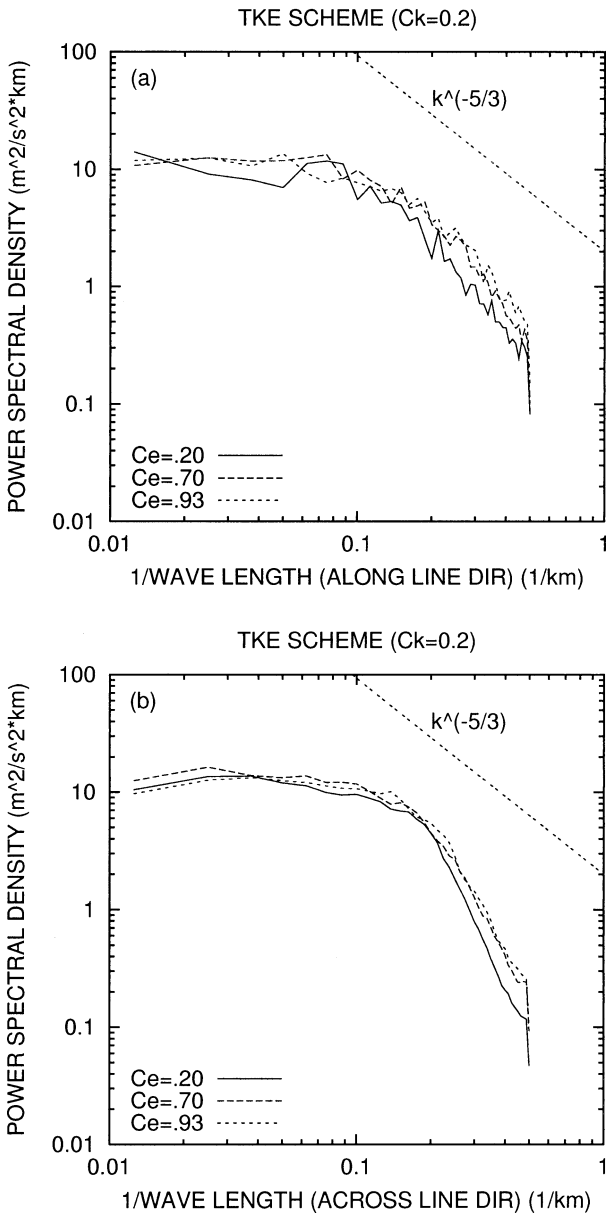

FIG. 10. Power spectral density of vertical velocity at the 3-km level for (a) along-line (y) and (b) across-line (x) directions obtained using the TKE scheme ($C_k = 0.2$) for various C_e values. A $k^{-5/3}$ line is also plotted for reference.

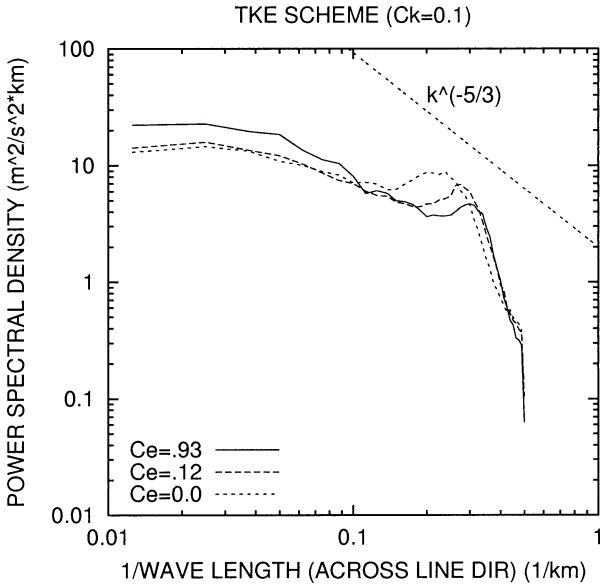

FIG. 11. Same as in Fig. 6 except for cases with the TKE scheme ($C_k = 0.1$) along with $C_e = 0.93$, 0.12, and 0.

the mixing by the TKE scheme with base C_k has a small impact on the simulated field. This point is also confirmed by the comparison between Figs. 1c, 3, and 13c; smoothing by the numerical filter seems to be much stronger than that of the subgrid model.

Since adding the filters resulted in smoother cells, the simulations with the filter may appear to be satisfactory. However, examining the power spectra reveals the difference between the results with and without the filter. Figure 14 shows the power spectral densities of vertical velocity at the 3-km level in the across-line direction for the cases shown in Fig. 13. The result obtained employing the TKE scheme ($C_k = 0.2$ and $C_e = 0.93$) without any filter is also shown for comparison. Short wavelengths less than $10\Delta x$ are more rapidly damped with than without the filter. Even though in the no-filter case the eddy viscosity coefficient is increased by a factor of 2 from the base value, the power at these wavelengths is well retained. This suggests that numerical filters damp some physically based small-scale

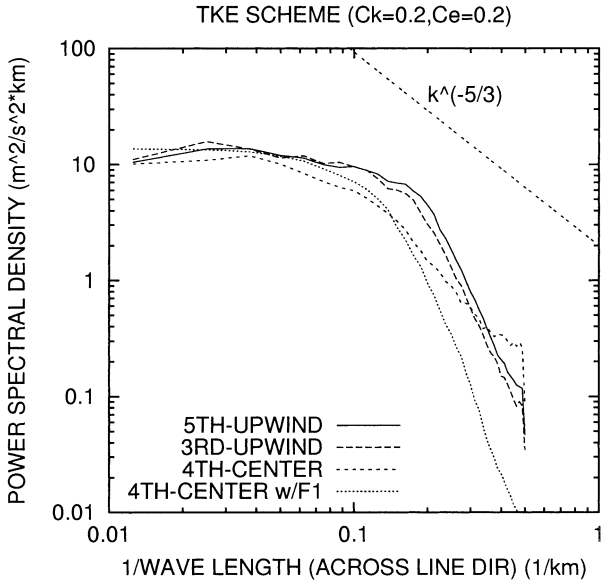

FIG. 12. Same as in Fig. 6 except for cases employing the TKE scheme ($C_k = 0.2$ and $C_e = 0.2$) obtained using the fifth-order and third-order upwind schemes, fourth-order centered scheme, and fourth-order centered scheme with the weak fourth-order filter.

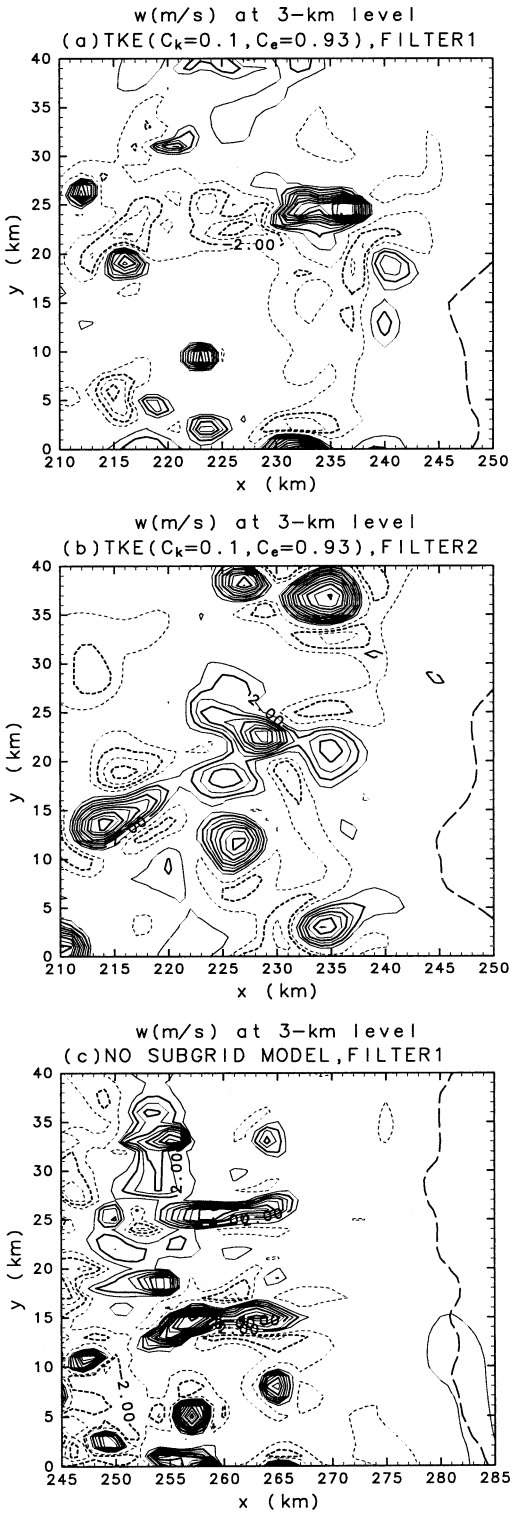

FIG. 13. Same as in Fig. 1 except for cases employing (a) the TKE scheme (C_k = 0.1, C_e = 0.93) and weak fourth-order filter, (b) the TKE scheme (C_k = 0.1, C_e = 0.93) and strong fourth-order filter, and (c) no subgrid model with the weak fourth-order filter.

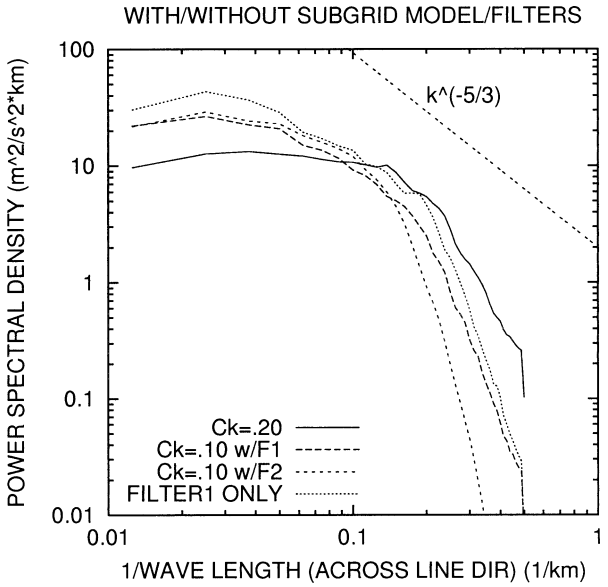

FIG. 14. Same as in Fig. 6 except for cases employing the TKE scheme (C_k = 0.2 and C_e = 0.93) (solid line); the TKE scheme (C_k = 0.1 and C_e = 0.93) with the weak filter (long-dashed line); the TKE scheme (C_k = 0.1 and C_e = 0.93) with the strong filter (short-dashed line); and only the weak filter without subgrid model (dotted line). A $k^{-5/3}$ line is plotted for reference.

eddies. It is noted that the power spectra appears to be larger at longer wavelengths ($>10\Delta x$) when the numerical filter is activated. This might be related to the subgrid model and filter formulations used here (the vertical eddy viscosity is equal to the horizontal one, while the numerical filter is applied only to the horizontal directions). However, we believe it unprofitable to discuss this point any further since we regard the filter as an artificial device to be avoided in future cloud model simulations.

Table 2 summarizes the domain total rainfall between 1 and 4 h obtained by using the TKE schemes (C_k = 0.1) in the weak- and strong-filter cases. The rain amounts in the FILTER1 cases are nearly the same as those obtained using the same C_k without filter (see Table 1). However, using FILTER2 the rain amounts increase over that in the no-filter cases. This result seems inconsistent with our expectation (based on Table 1) because the rainfall should decrease with increased filter strength. In Fig. 13b some well-organized cells are seen, and in Fig. 14 larger power can be found in long wavelengths more than $10\Delta x$ for the stronger filter; this seems

TABLE 2. Same as in Table 1 except for the TKE scheme (C_k = 0.1) with either weak (FILTER1) or strong (FILTER2) fourth-order filters.

Numerical filter	Total rainfall ($\times 10^{12}$ kg)		
	C_e = 0.2	C_e = 0.7	C_e = 0.93
FILTER1	0.114	0.130	0.134
FILTER2	0.141	0.154	0.156

to contribute the increased rainfall for the stronger filter case.

Comparing the results summarized in Tables 1 and 2, the rainfall varies very sensitively according to the filter strength and SGS constants C_s and C_k. We cannot tell which one is the best solution; however, it should be recognized that there is a strong sensitivity to filters and subgrid models. The characteristics of the explicit numerical filters as well as implicit filters in the third- and fifth-order advection schemes for a simple example are discussed in the appendix.

e. Sensitivities to grid spacing

From the earlier simulations we have found optimum values for C_s and C_k that give satisfactory solutions. However, the earlier simulations all employ a horizontal grid spacing of 1 km, and the dependence of the optimum SGS constants on grid spacing is still unknown. Thus, here we examine the sensitivities of simulations to horizontal grid spacing, employing the TKE scheme with one set of the optimum SGS constants, that is, (C_k, C_e) = (0.2, 0.93). As mentioned in section 2b, we examine horizontal grid spacings of 500 m, 2, and 4 km. The vertical grid spacing is the same as in the earlier simulations. No fourth-order numerical filter is added, and the fifth-order upwind-differencing scheme is used for the horizontal advection terms.

As in the above, we show here the horizontal cross section of vertical velocity at the 3-km level at 4 h (Fig. 15) and the power spectra of the vertical velocity at this level (Fig. 16a). For the 500-m-resolution case, the cells are well resolved. Increasing the grid spacing to 2 km, the gross features still look well resolved, even though some of the small-scale features as seen in Figs. 15a (500-m resolution) and 5b (1-km resolution) are not represented. Further increasing the grid spacing to 4 km, most of the cells seen in the finer-resolution simulations disappear; however, the solution seems to be tolerable in the sense that grid-scale features are not significant. Comparing the spectra, all the cases show no spurious buildup of energy at the shortest resolved scales, and the power for long scales (more than 10-km wavelength) shows no significant difference with each other. In addition, domain total rainfall during 1–4 h also shows no significant difference: 0.114, 0.0990, 0.0889, and 0.0985×10^{12} kg, respectively, for the 500-m-, 1-, 2-, and 4-km-resolution cases, although some fluctuations are noted.

We have also done resolution experiments using the base SGS constants (Fig. 16b). While less obvious, there is still an energy buildup at high wavenumbers in the highest-resolution experiment (Δx = 500 m); numerical simulations with a different model that uses the base SGS constants, but even higher resolution (Δx = 250 m), show evidence of similar grid-scale noise for the no-shear case (G. Bryan 2003, personal communication).

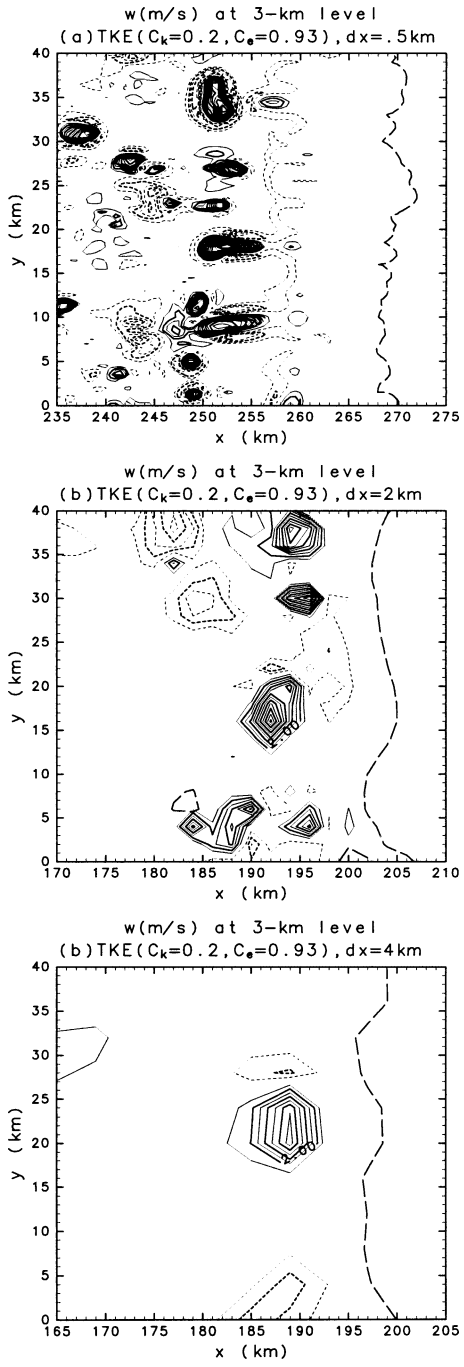

FIG. 15. Same as in Fig. 1 except for different horizontal grid spacings: (a) 500 m, (b) 2, and (c) 4 km.

From these simulations, we can conclude that the optimum SGS constants derived from the 1-km-resolution simulations are still valid for the grid spacing ranging from 500 m to 4 km.

4. Squall-line simulations in strong low-level shear

The earlier simulations were conducted in a no-shear environment. To examine the other limit of strong shear,

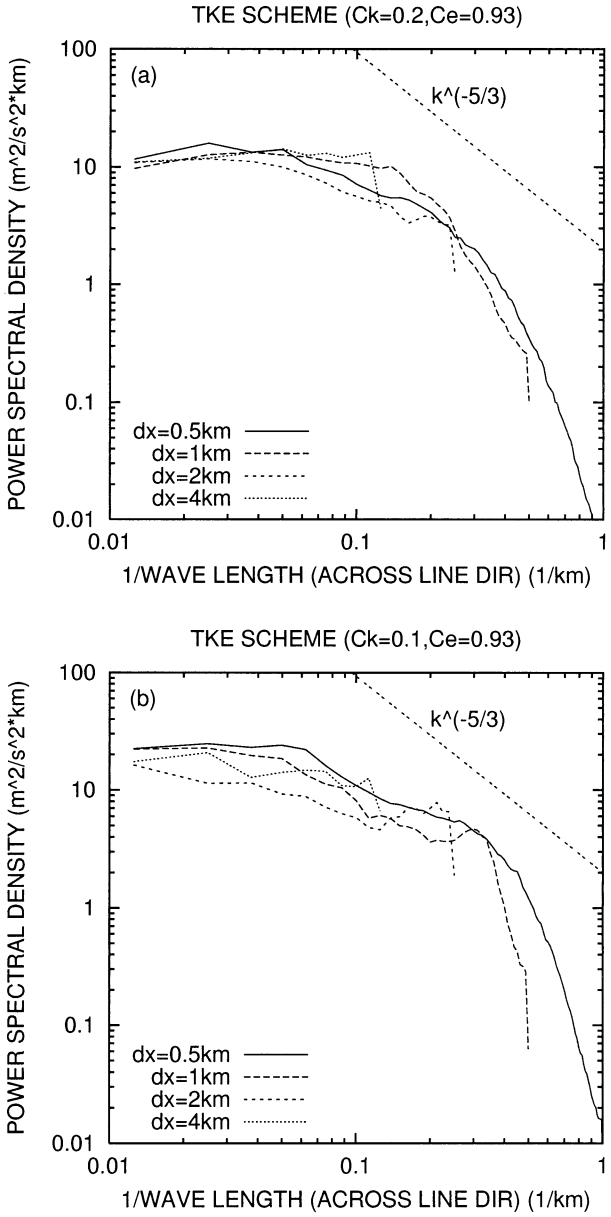

FIG. 16. Same as in Fig. 6 except for the cases of different horizontal grid spacings (500 m, 1, 2, and 4 km) using the TKE scheme with (a) $C_k = 0.2$ and $C_e = 0.93$, and (b) $C_k = 0.1$ and $C_e = 0.93$.

we impose a strong shear in the lowest levels, having an intensity of 20 m s^{-1} per 2.5 km. The effects of changing the constant C_k from 0.1 to 0.3 in the TKE scheme have been examined. In some of the larger C_k cases the initial thermal did not develop into an organized squall line probably because of increased diffusion.

Figure 17 shows the horizontal cross section of vertical velocity at the 3-km level, obtained by employing the TKE scheme ($C_k = 0.1$–0.25 and $C_e = 0.93$). The result using the base SGS value with FILTER1 is also demonstrated for comparison. Increasing the constant C_k the simulated field becomes more smoothed. In the $C_k = 0.1$ case grid-scale noise as seen in the no-shear cases appears to be suppressed; but this results from a stronger implicit filtering in the advection scheme due to a stronger flow field (see the appendix for the filter characteristics), and smaller-scale features can still be found as compared to the other four panels. The implicit filter appears to mask the problem found in the no-shear cases. Thus, in the strong-shear case the base SGS constant without a filter also seems to be inappropriate. The result obtained using the fourth-order filter (Fig. 17e) appears to be very smoothed without any small-scale features as seen in Figs. 17b,c (e.g., small-scale strong updrafts within the squall line). In Table 3, domain total rainfalls between 1 and 4 h are summarized for the shear simulations. Again, the rainfall decreases with increasing C_k. Smaller rainfall with smaller C_e at the same C_k is also identified as in the no-shear simulations. The simulated field using the filter appears to be the most smoothed among the cases shown in Fig. 17; however, comparing the total rainfall among the cases shown in Fig. 17 (see Table 3), the case with the filter is not excessively damped in the sense that the rainfall for this case is not so small as that obtained with $C_k \geq 0.15$. Similar to the no-shear simulations, the rainfall amount varies sensitively according to the filter strength and SGS constant.

Considering the simulated fields and rainfall amounts, a simulation with $C_k = 1.5 \sim 0.2$ gives a satisfactory solution. The result with $(C_k, C_e) = (0.25, 0.93)$ seems to be a little smoothed (Fig. 17d), and the total rain in this case is significantly reduced from that obtained using $C_k \leq 0.2$ (Table 3). In the no-shear simulation the combination of $C_k = 0.25$ and $C_e = 0.93$ gave a satisfactory result, but in strong-shear cases this combination is not appropriate.

5. Discussion

From a series of simulations presented here, we have demonstrated the sensitivities of the simulated squall lines to the SGS constants C_s, C_k, and C_e as well as numerical filters. The results obtained with both the Smagorinsky and TKE schemes have shown that there is an optimum value for C_s and C_k at which the simulated cells are well resolved. We have found that the results obtained with $C_s = 0.25 \sim 0.3$ for the Smagorinsky scheme and with $C_k = 0.15 \sim 0.2$ for the TKE scheme give satisfactory solutions. Smaller C_s and C_k result in widespread grid-scale features, and larger C_s and C_k result in excessively smoothed cells. This sensitivity has been found in both no-shear and strong-shear simulations. This kind of sensitivity to C_s was demonstrated by Mason and Callen (1986), Mason (1994), and Mason and Brown (1999) in their studies of large-eddy simulations of turbulent and boundary layer flows. We believe that by examining the effects of subgrid mixing and numerical filters the same reasoning as Mason's

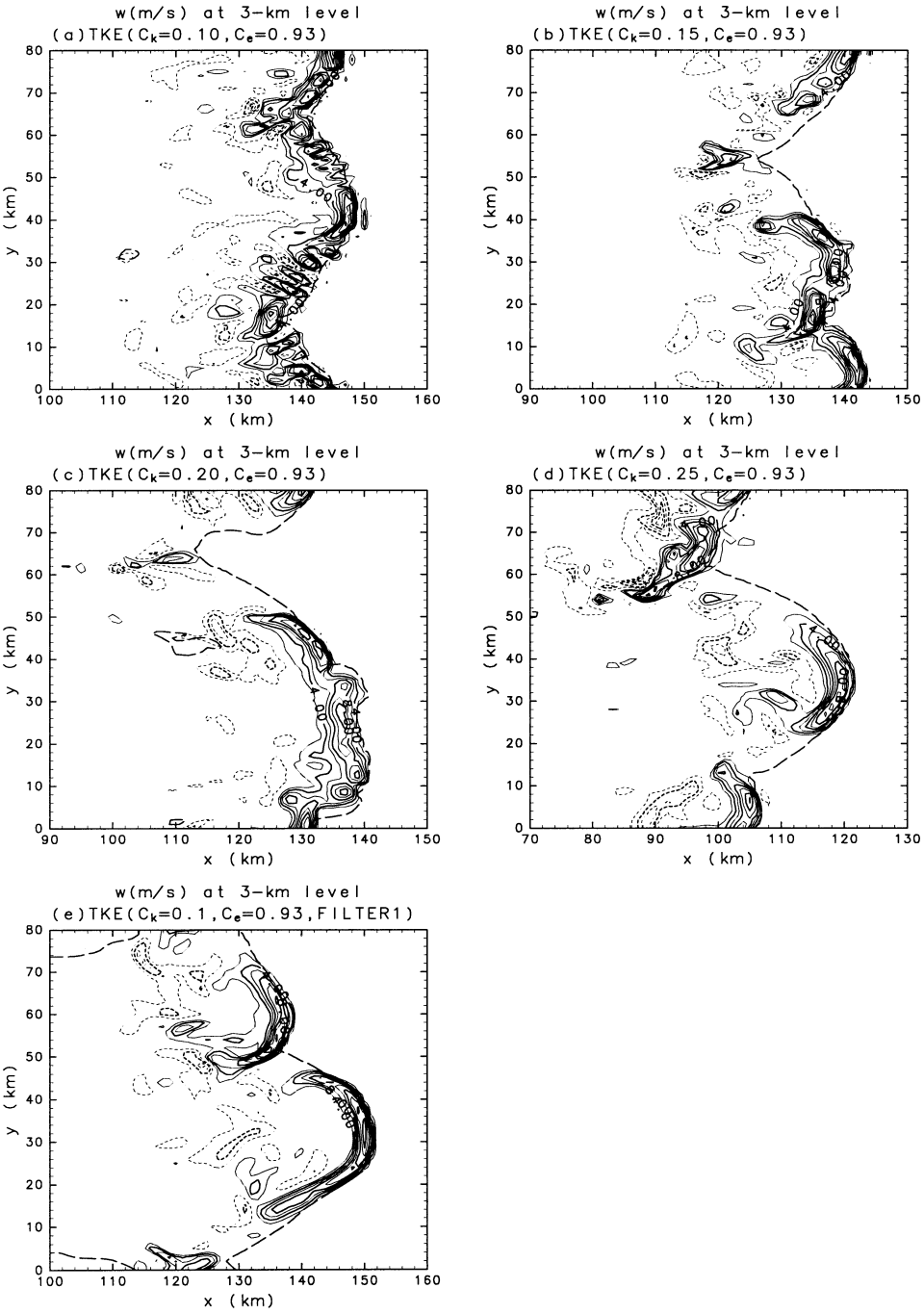

FIG. 17. Same as in Fig. 1 except for strong-shear cases (linear shear of 20 m s^{-1} over the lowest 2.5 km) and contoured at a 2 m s^{-1} interval, using TKE scheme with $C_e = 0.93$ and (a) $C_k = 0.1$, (b) $C_k = 0.15$, (c) $C_k = 0.2$, (d) $C_k = 0.25$, and (e) $C_k = 0.1$ with a weak fourth-order filter. A 60 km by 80 km portion of the entire domain is shown.

(1994) can be applied to the present results. It is noted that the present cloud simulations have used a relatively large grid spacing, probably well beyond the inertial subrange, as compared with grid spacings of large-eddy simulations. However, for lack of a better alternative these turbulence-closure schemes will continue to be used; the present study explores some of the consequences of using these schemes with commonly used parameter settings.

Using Eq. (5) we can define an effective Smagorinsky constant $C_{s\,\mathrm{eff}}$ in terms of the TKE constants C_k and C_e. Through this relationship, increasing C_k or decreasing

TABLE 3. Same as Table 1 except for the strong shear cases with the TKE schemes. The results obtained with FILTER1 (F1) are also shown for comparison.

	Total rainfall ($\times 10^{12}$ kg)	
C_k	$C_e = 0.2$	$C_e = 0.93$
0.1	0.189	0.198
0.15	0.174	0.174
0.2	0.149	0.175
0.25	0.0	0.0962
0.3	0.0	0.0
0.1 (w/F1)	0.186	0.184

C_e corresponds to increasing $C_{s\,\mathrm{eff}}$. Thus, the smoother cells found in smaller C_e or larger C_k cases can be interpreted by the increase of $C_{s\,\mathrm{eff}}$. Considering the effective Smagorinsky constant of the TKE scheme, larger C_k will be appropriate when choosing larger C_e. Thus, the recommendation can be made as to the choice of the appropriate TKE constants: $C_k \sim 0.15$ would be the best choice when C_e is set to 0.2 (yielding $C_{s\,\mathrm{eff}} = 0.36$); and $C_k \sim 0.2$ would be reasonable when $C_e = 0.93$ (yielding $C_{s\,\mathrm{eff}} = 0.30$). This is supported by the fact that the rainfall in the case with $C_k = 0.15$ and $C_e = 0.2$ agrees well with that in the $C_k = 0.2$ and $C_e = 0.93$ case in both the no-shear and strong-shear experiments (Tables 1 and 3), and also supported by a good agreement between the power spectra of these two combinations. On the other hand, the dependence of the simulations on C_e is much smaller than that on C_k; the use of very small C_e, even $C_e = 0$, still results in erroneous features when C_k is set to 0.1 (base constant). Thus, values of C_k larger than the base (commonly used) value is required in order for the simulations to be free of poorly resolved features. As Mason (1994), Canuto and Cheng (1997), and Mason and Brown (1999) pointed out, the proportionality constant C_s is not a universal constant. Likewise, the constants C_k and C_e should also be determined in order to obtain a satisfactory solution for each simulation. We have also examined sensitivities of the simulations using the earlier recommended SGS constants to horizontal grid spacing and found a set of values C_s, C_k, C_e that are adequate for grid spacing O(1 km). This is consistent with Mason and Brown's result: at a coarse resolution larger C_s gives a more satisfactory solution.

The previous studies using cloud models have not noticed the sensitivity to the SGS constants, because most cloud models had to use an artificial numerical filter to smooth out small-scale perturbations. However, as we have shown here, the mixing by numerical filters has a significant influence on the simulated fields. This sensitivity was noticed in previous studies (Lilly and Jewett 1990; Weisman et al. 1997), but not investigated systematically. Using the TKE scheme with the widely used $C_k = 0.1$, the subgrid model mixing has an effect much smaller than that of the numerical filter. As Mason (1994) argued, results with smaller C_s are liable to suffer from finite-difference errors. Thus, we consider that the base SGS constants, $C_s = 0.2$ and $C_k = 0.1$, are too small for the present simulations to be free from erroneous features. In order for subgrid mixing to dominate the grid-scale errors and in order not to use numerical filters, the constants C_s and C_k should be increased from the widely used values.

Mason (1994) suggested that the solutions would be insensitive to numerical methods (finite-differencing schemes) if $C_s \geq 0.2$. Our results using different upwind schemes also showed the small difference between the two schemes (Fig. 12); however, using the higher-order scheme seems to be more satisfactory in terms of the power spectra. Kravchenko and Moin (1997) concluded that the results of large-eddy simulations and the performance of a subgrid model is improved by increasing the order of the finite-difference scheme. Glendening and Haack (2001) argued that using a finer grid resolution is less computationally efficient than the use of a more accurate differencing scheme, even though accuracy can be increased with a finer grid resolution. Thus, it would be highly efficient to use the fifth-order upwind-differencing scheme along with a turbulent-closure model having the SGS constants that are appropriate for the simulations of grid spacing O(1 km).

6. Summary and conclusions

Using the Weather Research and Forecasting (WRF) model, which can be run stably without any explicit artificial filters, we have been able to separate the subgrid mixing and numerical filtering and perform systematically a series of squall-line simulations to examine the various effects of changing the proportionality constants C_s, C_k, and C_e in the Smagorinsky and TKE schemes as well as changing the strength of an added numerical filter. To our knowledge, this is the first attempt to study systematically such effects in cloud models.

Using the combination of the fifth-order upwind scheme for the advection terms and the TKE scheme with $C_k = 0.1$ (which is a widely used value for the simulations of planetary boundary layers and mesoscale cloud systems), many poorly resolved grid-scale cells were obtained in simulations of clouds in a no-shear environment. A common way to control such noise is to add artificial filters; however, these filters cannot separate the physical modes and computational noise. Thus, in some cases physically important small-scale features are damped. This is certainly not a desirable choice and may affect the development of convective cells in squall lines. This leads us to seek another way to control numerical errors and rely more on the subgrid model mixing.

Following Mason (1994), we have performed a series of simulations and found that the simulations with smaller C_s and C_k produce solutions with much grid-scale noise while those with larger C_s and C_k give ex-

cessively smoothed cells. There are optimum values for C_s and C_k in between: $C_s = 0.25 \sim 0.3$ for the Smagorinsky scheme, and $C_k \sim 0.15$ with $C_e = 0.2$ and $C_k \sim 0.2$ with $C_e = 0.93$ for the TKE scheme. With these values, the subgrid mixing dominates numerical errors and no additional numerical filters are required. We have also found that the subgrid mixing using the widely used C_s and C_k values has an effect much smaller than the numerical filtering using standard values for the filter coefficients.

The choice for the C_s and C_k values recommended here is empirical and the validity of those values should be evaluated in the future by direct numerical simulations with much finer grid spacing. While we cannot know the best choice of the SGS constants for cloud simulations, we have been able to exclude the obviously bad choices. The present work shows that these choices, along with numerics that have implicit diffusion, allow simulations of cloud systems without artificial numerical filters.

Acknowledgments. We would like to thank Drs. Joseph Klemp, Morris Weisman, and William Skamarock for many helpful suggestions and discussions. The comments by two anonymous reviewers and Dr. George Bryan were greatly appreciated for improving the original manuscript. This work has been done during the first author's visit to NCAR, which was supported partly by the Ministry of Education of Japan and partly by NCAR.

APPENDIX

Explicit and Implicit Numerical Filters

Described here are the formulations and characteristics of the fourth-order explicit filter and the implicit filter of the third- and fifth-order upwind-differencing schemes used in the present experiments. Both the explicit filter and the implicit filter of the upwind-biased advection schemes used in the WRF model (Wicker and Skamarock 2002) can be analyzed using the one-dimensional finite-difference equation,

$$\phi_j^{m+1} = \phi_j^m + (-1)^{n/2+1}\alpha\delta_n\phi_j, \tag{A1}$$

where ϕ_j^m denotes the value of the dependent variable ϕ at grid point j and time level m, and n is the order of the spatial filter $\delta_n\phi_j$. As described in Wicker and Skamarock (2002), the odd-order upwind-based advection schemes contain an implicit spatial filter of the next higher-order (e.g., $n = 4$ for the third-order upwind scheme); the filter constants are $\alpha = C_r/12$ and $C_r/60$ for the third- and fifth-order schemes, respectively, where $C_r(=U\Delta t/\Delta x)$ is the Courant number, $U(>0)$ is the local flow speed, Δt the time step and Δx the grid spacing. In the case of an explicit nth-order filter, $\alpha = (\gamma_n\Delta t)/(\Delta x)^n$, where γ_n is an arbitrarily chosen constant. The form of (A1) assumes n is even and so $\delta_n\phi_j$ for $n = 2, 4, 6$ may be written as

$$\delta_n\phi_j = \begin{cases} \phi_{j+1} - 2\phi_j + \phi_{j-1} & \text{(2nd order)} \\ \phi_{j-2} - 4\phi_{j-1} + 6\phi_j - 4\phi_{j+1} + \phi_{j+2} & \text{(4th order)} \\ \phi_{j-3} - 6\phi_{j-2} + 15\phi_{j-1} - 20\phi_j + 15\phi_{j+1} - 6\phi_{j+2} + \phi_{j+3} & \text{(6th order).} \end{cases} \tag{A2}$$

To investigate the damping characteristics of the various filters, we substitute into (A1) a single wave solution of the form $\phi_j^m = A^m \exp(ikj\Delta x)$, where k is the wavenumber, and obtain

$$\frac{A^{m+1}}{A^m} = 1 - 2\alpha(2 - 2\cos k\Delta x)^{n/2}. \tag{A3}$$

The properties of the amplification (damping) factor A^{m+1}/A^m are discussed in Durran (1999, p. 84, Fig. 2.15); in general, the higher the order of the filter, the less excessive damping there is on the resolved scales. However, even a higher-order filter produces excessive damping of the resolved scales if the filter coefficient is too large. Since the coefficients α of the implicit filters are a function of the Courant number, their filtering effects depend strongly on the local flow field. We examine here the effects of the implicit filters by using coefficients α typical of the simulated range of velocities (1–10 m s^{-1}) found in the no-shear experiments, and compare them with the damping effect of the explicit fourth-order filter employed in the present study. Using $\Delta x = 1000$ m and $\Delta t = 6$ s (as in the main body of simulations examined in this study) we investigate the effects of the implicit filter for cases with $C_r = 0.006$, 0.03, and 0.06 (corresponding to $U = 1$, 5, 10 m s^{-1}). For the explicit fourth-order filter we take $\gamma_4 = 4.0 \times 10^8$, which implies that $\alpha = 2.4 \times 10^{-3}$ ($=K_4$, referred to as FILTER1 in the main text). Figure A1 contains a graph of (A3) for the various cases discussed. Figure A1a shows that the implicit sixth-order filter has less damping in scales larger than $4\Delta x$ than the explicit filter for all U (i.e., for all α, where $\alpha = C_r/60 = 0.1$, 0.5, 1.0×10^{-3} corresponding to $U = 1$, 5, 10 m s^{-1}). However, Fig. A1b shows that the damping due to the implicit fourth-order filter ($\alpha = C_r/12 = 0.5$, 2.5, 5.0×10^{-3} corresponding to $U = 1$, 5, 10 m s^{-1}) becomes stronger than that of the explicit filter if $U > 5$ m s^{-1}.

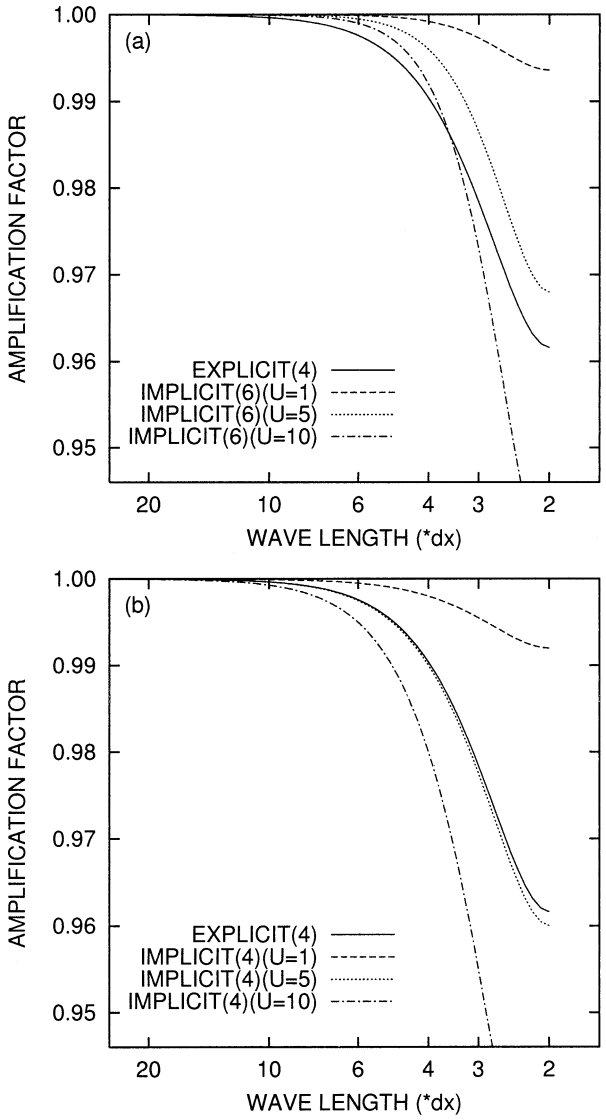

FIG. A1. Amplification factor for a weak fourth-order filter (solid line), and (a) implicit sixth-order filters in the fifth-order advection scheme and (b) implicit fourth-order filters in the third-order scheme. The cases of the implicit filters with velocities of 1, 5, and 10 m s^{-1} are indicated.

Thus, the use of the third-order advection scheme (which implies an implicit fourth-order filter) can cause significant damping in strong-wind cases. In the experiments with ambient wind shear, local velocities often exceed 10 m s^{-1}, and so the implicit and explicit filters have virtually the same effect.

REFERENCES

Canuto, V. M., and Y. Cheng, 1997: Determination of the Smagorinsky–Lilly constant C_s. *Phys. Fluids,* **9,** 1368–1378.

Deardorff, J. W., 1972: Numerical investigation of neutral and unstable planetary boundary layers. *J. Atmos. Sci.,* **29,** 91–115.

——, 1980: Stratocumulus-capped mixed layers derived from a three-dimensional model. *Bound.-Layer Meteor.,* **18,** 495–527.

Durran, D. R., 1999: *Numerical Methods for Wave Equations in Geophysical Fluid Dynamics.* Springer-Verlag, 465 pp.

Glendening, J. W., and T. Haack, 2001: Influence of advection differencing error upon large-eddy simulation accuracy. *Bound.-Layer Meteor.,* **98,** 127–153.

Hodur, R. M., 1997: The Naval Research Laboratory's Coupled Ocean/Atmosphere Mesoscale Prediction System (COAMPS). *Mon. Wea. Rev.,* **125,** 1414–1430.

Klemp, J. B., and R. B. Wilhelmson, 1978: The simulation of three-dimensional convective storm dynamics. *J. Atmos. Sci.,* **35,** 1070–1096.

Kravchenko, A. G., and P. Moin, 1997: On the effect of numerical errors in large eddy simulations of turbulent flows. *J. Comput. Phys.,* **131,** 310–322.

Lilly, D. K., 1962: On the numerical simulation of buoyant convection. *Tellus,* **14,** 148–172.

——, 1966: On the application of the eddy viscosity concept in the inertial sub-range of turbulence. Manuscript 123, National Center for Atmospheric Research, Boulder, CO, 19 pp.

——, and B. F. Jewett, 1990: Momentum and kinetic energy budgets of simulated supercell thunderstorms. *J. Atmos. Sci.,* **47,** 707–726.

Mason, P. J., 1994: Large-eddy simulation: A critical review of the technique. *Quart. J. Roy. Meteor. Soc.,* **120,** 1–26.

——, and N. S. Callen, 1986: On the magnitude of the subgrid-scale eddy coefficient in large-eddy simulations of turbulent channel flow. *J. Fluid Mech.,* **162,** 439–462.

——, and A. R. Brown, 1999: On subgrid models and filter operations in large eddy simulations. *J. Atmos. Sci.,* **56,** 2101–2114.

Moeng, C.-H., 1984: A large-eddy-simulation model for the study of planetary boundary-layer turbulence. *J. Atmos. Sci.,* **41,** 2052–2062.

——, and J. C. Wyngaard, 1988: Spectral analysis of large-eddy simulations of the convective boundary layer. *J. Atmos. Sci.,* **45,** 3573–3587.

Pope, S. B., 2000: *Turbulent Flows.* Cambridge University Press, 771 pp.

Rotunno, R., J. B. Klemp, and M. L. Weisman, 1988: A theory for strong, long-lived squall lines. *J. Atmos. Sci.,* **45,** 463–485.

Skamarock, W. C., and J. B. Klemp, 1992: The stability of time-split numerical methods for the hydrostatic and nonhydrostatic elastic equations. *Mon. Wea. Rev.,* **120,** 2109–2127.

——, ——, and J. Dudhia, 2001: Prototypes for the WRF (Weather Research and Forecasting) model. Preprints, *Ninth Conf. on Mesoscale Processes,* Fort Lauderdale, FL, Amer. Meteor. Soc., J11–J15.

Sullivan, P. P., J. C. McWilliams, and C.-H. Moeng, 1994: A subgrid-scale model for large-eddy simulation of planetary boundary-layer flows. *Bound.-Layer Meteor.,* **71,** 247–276.

Weisman, M. L., and J. B. Klemp, 1982: The dependence of numerically simulated convective storms on wind shear and buoyancy. *Mon. Wea. Rev.,* **110,** 504–520.

——, and R. Rotunno, 2001: The role of low-level vertical wind shear in promoting strong, long-lived squall lines. Preprints, *Ninth Conf. on Mesoscale Processes,* Fort Lauderdale, FL, Amer. Meteor. Soc., 298–302.

——, J. B. Klemp, and R. Rotunno, 1988: Structure and evolution of numerically simulated squall lines. *J. Atmos. Sci.,* **45,** 1990–2013.

——, W. C. Skamarock, and J. B. Klemp, 1997: The resolution dependence of explicitly modeled convective systems. *Mon. Wea. Rev.,* **125,** 527–548.

Wicker, L. J., and W. C. Skamarock, 2002: Time splitting methods for elastic models using forward time schemes. *Mon. Wea. Rev.,* **130,** 2088–2097.

Xue, M., K. K. Droegemeier, V. Wong, A. Shapiro, and K. Brewster, 1995: Advanced Regional Prediction System Version 4.0 User's Guide. Center for Analysis and Prediction of Storms, 380 pp. [Available from the Center for Analysis and Prediction of Storms, University of Oklahoma, Norman, OK 73019.]